JACS
JOURNAL OF THE AMERICAN CHEMICAL SOCIETY

ARTICLE

pubs.acs.org/JACS

Four-Coordinate, 14-Electron Ru^{II} Complexes: Unusual Trigonal Pyramidal Geometry Enforced by Bis(phosphino)silyl Ligation

Morgan C. MacInnis,[†] Robert McDonald,[‡] Michael J. Ferguson,[‡] Sven Tobisch,[*,§] and Laura Turculet[*,†]

[†]Department of Chemistry, Dalhousie University, Halifax, Nova Scotia B3H 4J3, Canada

[‡]X-ray Crystallography Laboratory, Department of Chemistry, University of Alberta, Edmonton, Alberta T6G 2G2, Canada

[§]School of Chemistry, University of St. Andrews, St. Andrews, Fife, KY16 9ST, United Kingdom

S Supporting Information

ABSTRACT: Unprecedented diamagnetic, four-coordinate, formally 14-electron (Cy-PSiP)RuX (Cy-PSiP = [κ^3-(2-$R_2PC_6H_4)_2SiMe]^-$; X = amido, alkoxo) complexes that do not require agostic stabilization and that adopt a highly unusual trigonal pyramidal coordination geometry are reported. The tertiary silane [(2-$Cy_2PC_6H_4)_2$SiMe]H ((Cy-PSiP)H) reacted with 0.5 [(*p*-cymene)$RuCl_2]_2$ in the presence of Et_3N and PCy_3 to afford [(Cy-PSiP)RuCl]$_2$ (**1**) in 74% yield. Treatment of **1** with KO^{t}Bu led to the formation of (Cy-PSiP)RuO^{t}Bu (**2**, 97% yield), which was crystallographically characterized and shown to adopt a trigonal pyramidal coordination geometry in the solid state. Treatment of **1** with NaN(SiMe$_3$)$_2$ led to the formation of (Cy-PSiP)RuN(SiMe$_3$)$_2$ (**3**, 70% yield), which was also found to adopt a trigonal pyramidal coordination geometry in the solid state. The related anilido complexes (Cy-PSiP)RuNH(2,6-$R_2C_6H_3$) (**4**, R = H; **5**, R = Me) were also prepared in >90% yields by treating **1** with LiNH(2,6-$R_2C_6H_3$) (R = H, Me) reagents. The solid state structure of **5** indicates a monomeric trigonal pyramidal complex that features a C−H agostic interaction. Complexes **2** and **3** were found to react readily with 1 equiv of H_2O to form the dimeric hydroxo-bridged complex [(Cy-PSiP)RuOH]$_2$ (**6**, 94% yield), which was crystallographically characterized. Complexes **2** and **3** also reacted with 1 equiv of PhOH to form the new 18-electron η^5-oxocyclohexadienyl complex (Cy-PSiP)Ru(η^5-C_6H_5O) (**7**, 84% yield). Both amido and alkoxo (Cy-PSiP)RuX complexes reacted with $H_3B\cdot NHRR'$ reagents to form bis(σ-B−H) complexes of the type (Cy-PSiP)RuH(η^2:η^2-H_2BNRR') (**8**, R = R′ = H; **9**, R = R′ = Me; **10**, R = H, R′ = ^{t}Bu), which illustrates that such four-coordinate (Cy-PSiP)RuX (X = amido, alkoxo) complexes are able to undergo multiple E−H (E = main group element) bond activation steps. Computational methods were used to investigate structurally related PCP, PPP, PNP, and PSiP four-coordinate Ru complexes and confirmed the key role of the strongly σ-donating silyl group of the PSiP ligand set in enforcing the unusual trigonal pyramidal coordination geometry featured in complexes **2**−**5**, thus substantiating a new strategy for the synthesis of low-coordinate Ru species. The mechanism of the activation of ammonia-borane by such low-coordinate (R-PSiP)RuX (X = amido, alkoxo) species was also studied computationally and was determined to proceed most likely in a stepwise fashion via intramolecular deprotonation of ammonia and subsequent borane B−H bond oxidative addition steps.

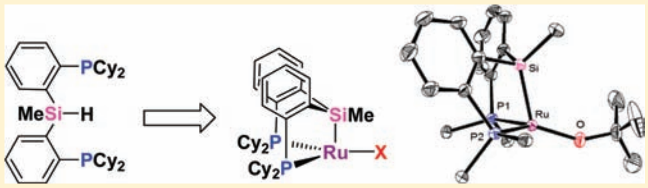

INTRODUCTION

Coordinatively and electronically unsaturated late transition metal complexes that feature less than 16 valence electrons are invoked as key intermediates in numerous stoichiometric and catalytic metal-mediated processes.[1] Although there is significant interest in the preparation and study of such complexes to better understand their role in organometallic reactivity, their isolation is typically thwarted by their highly reactive nature. As such, the identification of strategies for the preparation of isolable transition metal complexes that formally feature less than 16 valence electrons continues to attract significant interest. In the case of Ru^{II}, most isolated complexes are either five- or six-coordinate species that feature 16- or 18-electron configurations, respectively.[2] In contrast, crystallographically characterized four-coordinate, formally 14-electron Ru^{II} complexes are exceedingly rare[3−5] and with few exceptions[3,4] feature the presence of stabilizing C−H agostic interactions[15] that facilitate their isolation. Notably, Caulton and co-workers have reported the unusual square planar, 14-electron Ru^{II} complex ((^{t}Bu$_2$PCH$_2$SiMe$_2$)$_2$N)RuCl that does not feature agostic stabilization as a consequence of adopting a triplet spin state.[3a] More recently, Schneider and co-workers reported the synthesis of the closely related square planar complex ((^{t}Bu$_2$PCH$_2$CH$_2$)$_2$N)RuCl that adopts a singlet ground state as a result of increased π-donation from the chelating dialkyl amido ligand, relative to the disilyl amido ligand featured in Caulton's complex.[3c] Given the rarity of formally 14-electron Ru^{II} complexes devoid of agostic stabilization and the insights that might be obtained through the systematic study of such species, the development of new strategies for the

Received: May 29, 2011
Published: August 10, 2011

Scheme 1. Synthesis of (Cy-PSiP)RuX (X = Amido, Alkoxo) Complexes

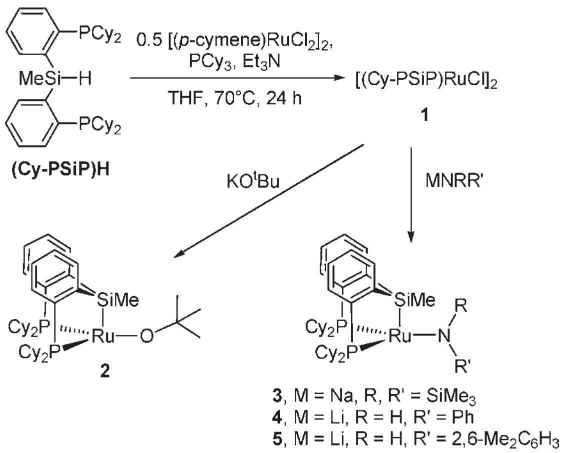

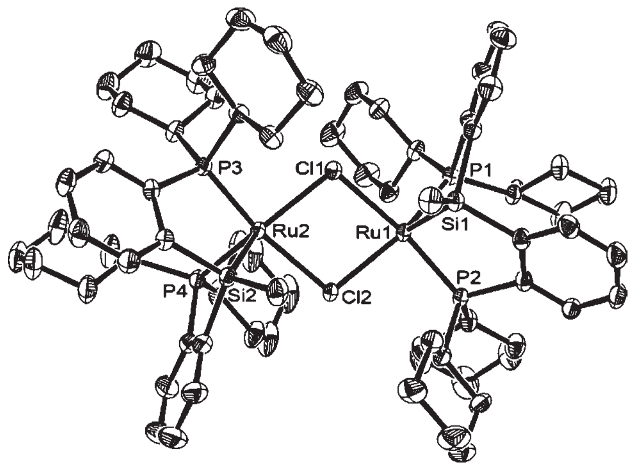

Figure 1. Crystallographically determined structure of $1 \cdot 3.5C_6H_6$ shown with 50% ellipsoids. H atoms and the C_6H_6 solvate have been omitted for clarity. Selected interatomic distances (Å) and angles (deg): Ru1−Cl1 2.4597(7), Ru1−Cl2 2.4591(7), Ru1−Si1 2.2770(8), Ru2−Cl1 2.4815(7), Ru2−Cl2 2.4748(7), Ru2−Si2 2.2733(8), P1−Ru1−P2 97.05(3), and P3−Ru2−P4 96.52(3).

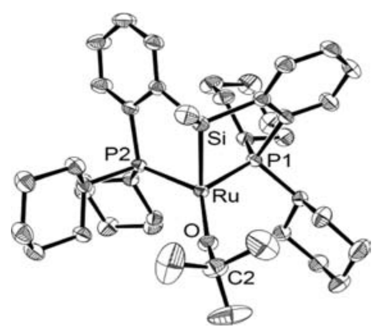

Figure 2. Crystallographically determined structure of $2 \cdot C_6H_6 \cdot 0.5 C_5H_{12}$ shown with 50% ellipsoids. H atoms and the C_6H_6 and C_5H_{12} solvates have been omitted for clarity. Selected interatomic distances (Å) and angles (deg): Ru−Si 2.2859(6), Ru−O 1.9090(14), P1−Ru−P2 99.25(2), P1−Ru−O 127.21(5), P2−Ru−O 129.16(5), and Si−Ru−O 119.03(5).

synthesis of unsaturated Ru complexes represents an important challenge. Moreover, the identification of new structural motifs in such low coordinate species is of particular significance, as examples that do not require agostic stabilization are currently limited to square planar species. The discovery of new classes of four-coordinate Ru^{II} complexes that adopt novel structures is anticipated to broaden our understanding of the electronic and steric factors underlying the preferred geometries of four-coordinate Ru^{II} complexes, as well as to provide access to new types of reactivity for such unsaturated species.

In this context, we have recently reported on the synthesis and reactivity of a variety of coordinatively unsaturated late transition metal complexes supported by new tridentate bis(phosphino)-silyl ligands of the type $[\kappa^3\text{-}(2\text{-}R_2PC_6H_4)_2SiMe]^-$ (R-PSiP, R = Ph, Cy),[6] including examples of pincer-like Ir species that can undergo facile intermolecular C−H and N−H bond activation chemistry,[6b,d] as well as a series of square planar Group 10 complexes that undergo unusual Si−C bond cleavage reactions.[6e] In building on these studies, we viewed tridentate bis(phosphino)-silyl ligation as providing an attractive entry point for the synthesis of low-coordinate Ru^{II} complexes, whereby both the steric demands of the phosphino substituents and the strongly *trans*-directing silyl group would enforce coordinative unsaturation. We report herein the isolation and solution/solid state characterization of diamagnetic, four-coordinate, formally 14-electron (Cy-PSiP)RuX (X = amido, alkoxo) complexes that do not require agostic stabilization and that adopt a highly unusual trigonal pyramidal coordination geometry. Computational studies confirm the key role of the strongly σ-donating silyl group of the Cy-PSiP ligand in enforcing this unusual geometry. While silyl ligation affords stability to the four-cordinate (Cy-PSiP)RuX complexes featured herein, these low-coordinate species are still capable of reacting with substrate E−H bonds, as demonstrated by their ability to undergo N−H/B−H bond activation upon treatment with amine-borane reagents.

RESULTS AND DISCUSSION

Synthesis and Structural Characterization of Four-Coordinate (Cy-PSiP)RuX Complexes. The reaction of the tertiary silane (Cy-PSiP)H with 0.5 $[(p\text{-cymene})RuCl_2]_2$ in the presence of Et_3N and PCy_3 afforded orange, diamagnetic $[(\text{Cy-PSiP})RuCl]_2$ (**1**) in 74% yield (Scheme 1). The solid state structure of **1** was determined by single-crystal X-ray diffraction analysis (Figure 1) and is consistent with the formulation of **1** as a dinuclear complex that features bridging chloride ligands. Solution and refinement parameters for each of the crystallographically characterized compounds reported herein are given in Table S1 (Supporting Information (SI)).

Complex **1** serves as a useful precursor for the synthesis of novel 14-electron (Cy-PSiP)RuX (X = amido, alkoxo) complexes. Thus, treatment of **1** with KO^tBu in benzene solution at room temperature led to the formation of red, diamagnetic (Cy-PSiP)RuO^tBu (**2**), which exhibits a single ^{31}P NMR resonance at 110.5 ppm. Complex **2** was readily isolated in 97% yield and is formulated as a monomeric, formally 14-electron species on the basis of solution NMR and X-ray diffraction data (Figure 2). Surprisingly, despite the prevalence of square planar and tetrahedral geometries for four-coordinate transition metal complexes, the solid state structure of **2** exhibits slightly distorted trigonal pyramidal coordination geometry at Ru, with Si in the

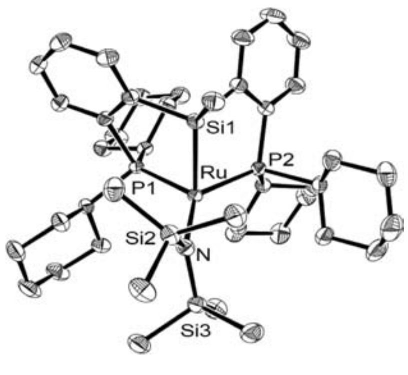

Figure 3. Crystallographically determined structure of **3** shown with 50% ellipsoids. H atoms have been omitted for clarity. Selected interatomic distances (Å) and angles (deg): Ru−Si1 2.3087(4), Ru−N 2.0465(12), P1−Ru−P2 97.341(14), P1−Ru−N 125.61(4), P2−Ru−N 134.75(4), and Si1−Ru−N 114.58(4).

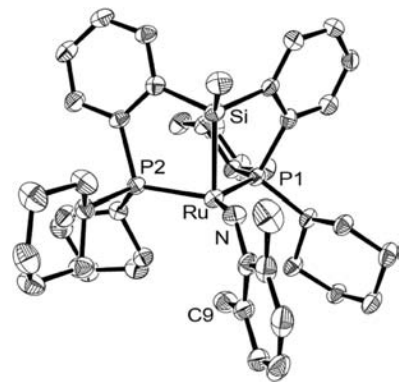

Figure 4. Crystallographically determined structure of **5** shown with 50% ellipsoids. Selected H atoms have been omitted for clarity. Selected interatomic distances (Å) and angles (deg): Ru−Si 2.2813(11), Ru−N 1.995(2), Ru···C9 2.749(3), P1−Ru−P2 100.26(4), P1−Ru−N 133.62(8), P2−Ru−N 125.46(8), and Si−Ru−N 93.21(8).

apical site. The sum of P1−Ru−P2 (99.25(2)°), P1−Ru−O (127.21(5)°), and P2−Ru−O (129.16(5)°) angles is 355.62°, which is very close to idealized trigonal planar geometry at Ru in the equatorial plane. Notably, no agostic interactions are apparent in the solid state structure of **2** (all Ru···C > 3 Å). The geometry at the O^{t}Bu ligand oxygen is bent (Ru−O−C2 = 152.0(2)°), and the Ru−O distance of 1.909(1) Å is statistically shorter than the analogous linkage found in Ru alkoxide complexes where Ru−O π-bonding has been invoked (e.g., 1.99(1) Å for Cp*Ru(PCy$_3$)(OCH$_2$CF$_3$)).[7]

The alkoxide complex **2** represents a rare example of a four-coordinate, formally 14-electron Ru^{II} complex. To the best of our knowledge, the only directly comparable species for which crystallographic data have been presented is (Cy$_3$P)(^{t}BuO)$_2$Ru=CHPh (Ru−O = 1.9412(15), 1.9558(15) Å), in which the phosphine ligand occupies the apical position of the trigonal pyramidal structure.[8,9] Conversely, the spin triplet 14-electron complex *trans*-Ru(^{t}Bu$_2$PCH$_2$SiMe$_2$O)$_2$ reported by Caulton and co-workers features square planar geometry.[3b] Interestingly, although mononuclear **2** can be viewed as being isoelectronic with Cp*RuOR, Cp*RuO^{t}Bu has been reported to be unstable,[10a] and complexes such as Cp*Ru(OCH$_2$CF$_3$) and Cp*Ru(OMe) are dimers in the solid state.[7,10b]

In an effort to further explore the synthesis of such four-coordinate (Cy-PSiP)RuX species, we also undertook the synthesis of related amido complexes. Thus, treatment of **1** with NaN(SiMe$_3$)$_2$ in benzene solution at room temperature led to the formation of dark red, diamagnetic (Cy-PSiP)RuN(SiMe$_3$)$_2$ (**3**, 70% yield), which exhibits a single ^{31}P NMR resonance at 98.9 ppm. The solid state structure of **3** (Figure 3) indicates a monomeric complex that, as in the case of complex **2**, exhibits a highly unusual, distorted trigonal pyramidal coordination geometry at Ru with Si in the apical site ($\Sigma_{PRuP,PRuN}$ = 357.70°). As in the case of **2**, no agostic interactions are apparent in the solid state structure of **3** (all Ru···C > 3 Å). The planar amido ligand ($\Sigma_{SiNSi,SiNRu}$ = 359.65°) is oriented perpendicular to the trigonal plane of the complex, with a Ru−N bond distance of 2.047(1) Å that is comparable to that observed for Caulton's square planar ((^{t}Bu$_2$PCH$_2$SiMe$_2$)$_2$N)RuCl (Ru−N = 2.050(1) Å),[3a] suggesting the possibility of π-donation from N to Ru. Notably, the Ru−N distance reported by Schneider and co-workers for the related square planar complex ((^{t}Bu$_2$PCH$_2$CH$_2$)$_2$N)RuCl, where significant Ru−N π-bonding is invoked, is much shorter at 1.890(2) Å.[3c]

The synthesis of related anilido complexes was also pursued by treating **1** with LiNH(2,6-R$_2$C$_6$H$_3$) (R = H, Me) reagents. The corresponding anilido complexes (Cy-PSiP)RuNH(2,6-R$_2$C$_6$H$_3$) (**4**, R = H; **5**, R = Me) were each isolated as dark red solids in >90% yield. Complexes **4** and **5** each exhibit a single ^{31}P NMR resonance at 96.5 and 94.2 ppm, respectively. In addition, the ^{1}H NMR spectra of **4** and **5** (benzene-d_6) each feature a broad resonance corresponding to the N*H* proton of the anilido ligand at 6.35 and 7.57 ppm, respectively. Although we were unable to obtain X-ray quality crystals of **4**, the solid state structure of **5** (Figure 4) indicates a monomeric complex that, as in the case of complexes **2** and **3**, exhibits slightly distorted trigonal pyramidal coordination geometry at Ru with Si in the apical site ($\Sigma_{PRuP,PRuN}$ = 359.34°). The Ru−N distance of 1.995(2) Å is somewhat shorter than the Ru−N distance in **3** and is considerably shorter than the Ru−N distances in the dimeric species [Cp*Ru-(μ-NHPh)]$_2$ (2.101(8) and 2.117(7) Å).[11] The anilido phenyl ring in **5** is oriented nearly perpendicular to the P$_2$RuN plane, as indicated by the Ru−N−C−C torsional angle of 175.9(2)°. This orientation positions a methyl substituent (C9) on the anilido ligand proximal to the empty coordination site trans to Si. The resulting short Ru···C9 distance of 2.749(3) Å is consistent with a C−H agostic interaction, the existence of which is authenticated by computational data (vide infra). The absence of stabilizing agostic interactions in complexes **2** and **3** suggests that such an interaction in **5** may result from the fortuitous positioning of an anilido methyl substituent arising from the sterically and/or electronically preferred orientation of the anilido ligand. The predisposition for such *ortho*-Me substituents to engage in agostic interactions due to their inherent proximity to a coordinatively unsaturated metal center has been previously documented for *ortho*-Me-substituted aryl phosphine ligands.[5d]

Reactivity Studies. In an effort to determine if complexes such as **2** and **3** could serve as precursors to new low-coordinate Ru species via protonolysis reactions, the reactivity of these complexes with reagents that feature relatively acidic O−H groups was probed. Our initial investigation explored the reactivity of **2** and **3** with H$_2$O and PhOH, as the corresponding hydroxo and phenoxo Ru complexes were not accessible via reactions of **1** with the corresponding alkali metal salts (MOH or MOPh, where M = alkali metal). Both **2** and **3** were found to react quantitatively (^{31}P NMR) with 1 equiv of degassed H$_2$O to

Scheme 2. Reactivity of Four-Coordinate (Cy-PSiP)RuX (X = O^{t}Bu, N(SiMe$_3$)$_2$) Complexes

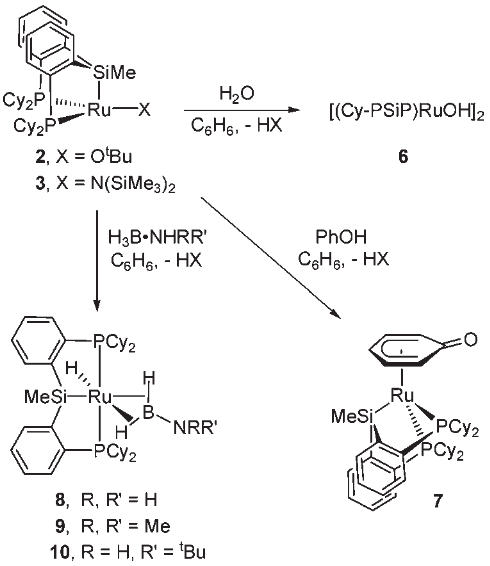

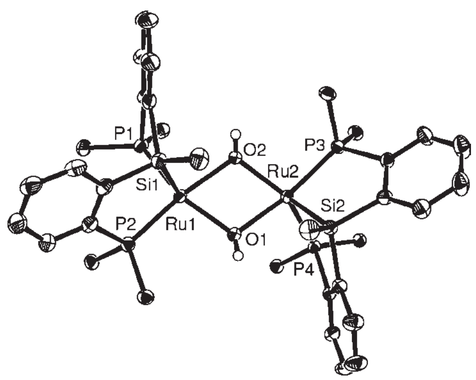

Figure 5. Crystallographically determined structure of $6 \cdot C_7H_8$ shown with 50% ellipsoids. Selected H and selected cyclohexyl C atoms, as well as the C_7H_8 solvate, have been omitted for clarity. Selected interatomic distances (Å) and angles (deg): Ru1−Si1 2.2647(12), Ru2−Si2 2.2692(12), Ru1−O1 2.079(3), Ru2−O1 2.124(3), Ru1−O2 2.115(3), Ru2−O2 2.070(3), P1−Ru1−P2 99.98(4), P3−Ru2−P4 101.11(4), O1−Ru1−O2 70.74(11), O1−Ru2−O2 70.74(11), Ru1−O1−Ru2 107.81(13), Ru1−O2−Ru2 108.43(13).

form the new dimeric hydroxo complex **6** (Scheme 2). The solid state structure of **6** (Figure 5) is similar to that previously observed for **1** and confirms the formation of a dinuclear Ru complex with bridging hydroxo ligands. Each Ru center features distorted square-based pyramidal coordination geometry, with Si occupying the apical site. The Ru−O distances in **6** (2.070(3) − 2.124(3) Å) are all significantly longer than the Ru−O distance of 1.909(1) Å observed for **2**. The dimeric nature of **6** relative to monomeric **2** confirms that steric bulk plays an important role in attaining a monomeric structure for complexes of the type (Cy-PSiP)-RuX. In room-temperature benzene solution, **6** exhibits inequivalent phosphorus environments on the NMR time scale, as evidenced by two equal-intensity $^{31}P\{^1H\}$ NMR resonances observed at 91.2 (d, $^2J_{PP}$ = 25 Hz) and 86.5 (d, $^2J_{PP}$ = 25 Hz) ppm. Coalescence of these resonances is observed upon warming, such

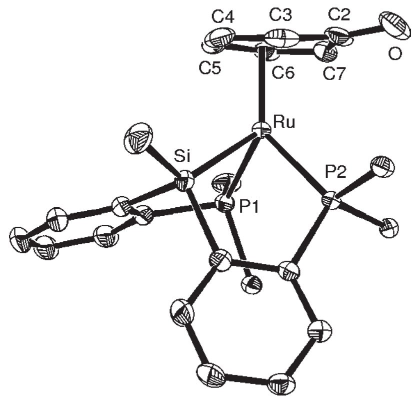

Figure 6. Crystallographically determined structure of $7 \cdot C_6H_6$ shown with 50% ellipsoids. H atoms and selected cyclohexyl C atoms, as well as the C_6H_6 solvate, have been omitted for clarity. Selected interatomic distances (Å) and angles (deg): Ru−Si 2.3276(6), O−C2 1.249(3), C2−C3 1.453(4), C2−C7 1.438(3), C3−C4 1.405(4), C4−C5 1.405(3), C5−C6 1.408(3), C6−C7 1.392(3), Ru−C2 2.582(2), Ru−C3 2.279(2), Ru−C4 2.217(2), Ru−C5 2.257(2), Ru−C6 2.320(2), Ru−C7 2.418(2), P1−Ru−P2 94.214(18), P1−Ru−Si 79.30(2), and P2−Ru−Si 82.985(19).

that a single ^{31}P NMR resonance (94.8 ppm) is observed for the complex at 363 K.

Complexes **2** and **3** were also observed to react quantitatively (^{31}P NMR) with 1 equiv of PhOH to form the new 18-electron η^5-oxocyclohexadienyl complex **7** (Scheme 2). The solid state structure of **7** (Figure 6) confirms the pentadienyl nature of the η^5-C_6H_5O ligand, as indicated by the short C−C bond distances within the pentadienyl ring (1.392(3)−1.408(3) Å) relative to the C−C bonds to C2 (C2−C3 1.453(4) Å, C2−C7 1.438(3) Å). The O−C2 distance of 1.249(3) Å is consistent with double bond character and is comparable to analogous distances previously reported for η^5-oxocyclohexadienyl complexes (e.g., 1.256(4) Å for Cp*Ru(η^5-2,6-^{t}Bu$_2$C$_6$H$_3$O)[10b] and 1.277 Å for Ru(H)(PPh$_3$)$_2$(η^5-C$_6$H$_5$O)·MeOH).[12] The phenyl ring is slightly folded such that the ipso carbon C2 is bent away from the Ru center, as indicated by examination of the least-squares planes. The ipso carbon and O atoms lie 0.191(3) and 0.419(4) Å, respectively, out of the plane defined by the pentadienyl carbon atoms (C3−C7). The angle between the pentadienyl plane and that defined by C2, C3, C7, and O is 11.84(9)°, which confirms the puckering of the C_6H_5O ligand. In solution, the protons of the η^5-C_6H_5O ring are observed at 5.62, 5.14, and 3.98 ppm; the upfield shift of these protons is comparable to that previously reported for related η^5-oxocyclohexadienyl complexes.[10b,12] The formation of this 18-electron π-type phenol complex parallels the chemistry observed for the Cp*Ru fragment, where π-complexation of phenol and most phenol derivatives, including perfluorinated phenols, is thermodynamically preferred and is observed almost exclusively.[10,13]

Our current efforts are aimed at exploring the bond activation chemistry of (R-PSiP)RuX complexes, such as those described herein, in an effort to evaluate how such coordinatively and electronically unsaturated complexes might be exploited in reactivity applications. In an initial survey of E−H (E = main group element) bond activation chemistry, complexes **2** and **3** were found to readily undergo multiple E−H bond activation steps upon treatment with 1 equiv of $H_3B \cdot NH_3$ to form quantitatively the bis(σ-B−H) complex (Cy-PSiP)RuH(η^2:η^2-H_2BNH_2) (**8**),

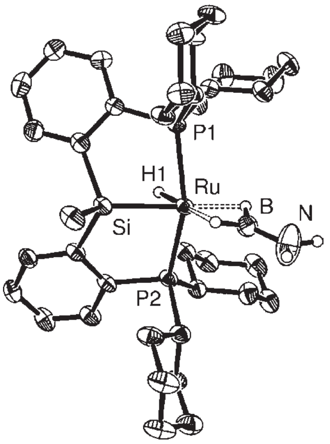

Figure 7. Crystallographically determined structure of **8** shown with 50% ellipsoids; selected H atoms have been omitted for clarity. Selected interatomic distances (Å) and angles (deg): Ru−Si 2.3276(14), Ru···B 2.031(6), B−N 1.359(8), P1−Ru−P2 155.22(5), and Ru−B−N 173.3(5).

with concomitant formation of either HO^tBu or $HN(SiMe_3)_2$, respectively (Scheme 2). Complex **8**, which represents a rare example of a bis(σ-B−H) aminoborane complex,[14] was readily isolated in 81% yield and has been characterized both in solution and in the solid state (Figure 7). Only one previous example of a crystallographically characterized bis(σ-B−H) complex of H_2BNH_2 has been recently reported by Alcaraz, Sabo-Etienne, and co-workers.[14a] The substituted amine-boranes $H_3B{\cdot}NHMe_2$ and $H_3B{\cdot}NH_2{}^tBu$ reacted in a similar manner (Scheme 2) to form the related bis(σ-B−H) complexes (Cy-PSiP)RuH(η^2:η^2-H_2BNMe_2) (**9**, Figure S1 in the SI) and (Cy-PSiP)RuH(η^2:η^2-H_2BNH^tBu) (**10**). Each of the complexes **8**−**10** feature two distinctive upfield shifted ^1H NMR resonances corresponding to the Ru−*H*−B protons that are observed as broad singlets at −3.36 and −7.50 ppm for **8**, −3.29 and −7.49 ppm for **9**, and −3.34 and −7.56 ppm for **10** (benzene-d_6). In addition, the ^1H NMR spectrum of each complex features a resonance corresponding to the terminal Ru−H ligand (−12.62 ppm for **8**, −13.07 ppm for **9**, and −12.66 ppm for **10**). The $^{11}B\{^1H\}$ NMR spectra of **8**−**10** feature a broad signal at ca. 40 ppm, which is characteristic of a three-coordinate boron atom and is comparable to the ^{11}B NMR shift of 46 ppm reported for $RuH_2(\eta^2{:}\eta^2\text{-}H_2BNH_2)(PCy_3)_2$.[14a] The X-ray structures of **8** and **9** indicate that in each case the Ru center adopts a pseudo-octahedral coordination environment featuring *trans*-disposed phosphino groups. The Ru···B distances of 2.031(6) and 2.021(2) Å are shorter than the sum of the covalent radii for Ru and B (2.09 Å)[14a,b] but are somewhat longer than the Ru···B distance of 1.956(2) Å reported for $RuH_2(\eta^2{:}\eta^2\text{-}H_2BNH_2)(PCy_3)_2$.[14a] The coordinated aminoborane ligand in both **8** and **9** features a short B−N distance (1.359(8) Å for **8** and 1.386(3) Å for **9**; cf. 1.58(2) Å for $H_3B{\cdot}NH_3$[15]) that is consistent with appreciable π-bonding character. Notably such bis(σ-B−H) complexes represent possible intermediates in the metal-mediated dehydrogenation of amine-boranes, including ammonia-borane, which has attracted significant attention as a hydrogen storage material.[14b,16,17] In this context, the formation of **8**−**10** from either **2** or **3** confirms that such four-coordinate, formally 14-electron (R-PSiP)RuX complexes are capable of promoting multiple bond activation steps in a manner that may be synthetically useful in the transformation of main group substrates.

Computational Studies. The experimental work was complemented by DFT (TPSS/SDD+TZVP)[18] studies of the structural and electronic features of the four-coordinate complexes **2**, **3**, and **5**. The DFT optimized structures in the singlet state were in excellent agreement with X-ray diffraction data (cf. Figure S2 in the SI).[18b] DFT confirmed the slightly distorted trigonal pyramidal geometry of the four-coordinate complexes **2**, **3**, and **5** featuring *fac*-κ^3-(Cy-PSiP)Ru^{II} ligation, whereby the alternative *mer*-κ^3-pincer−Ru^{II} coordination mode that is preferably adopted in a nonplanar *cis*-divacant octahedral geometry at Ru is higher in energy by 28.8 (**2**), 34.2 (**3**), and 32.0 (**5**) kcal mol^{-1}, respectively. The ability to establish Ru^{II}−X π interactions efficiently is a crucial factor that favors the *fac*-κ^3 over the *mer*-κ^3 ligation mode. Taking complex **2** as an example, optimized Ru−O distances of 1.91 and 1.98 Å for *fac*-κ^3 and *mer*-κ^3 forms, respectively, are indeed suggestive of stronger Ru^{II}−O π interactions in the former. The stability of the diamagnetic, four-coordinate, formally 14-electron (Cy-PSiP)RuX complexes reported herein cannot be attributed to a triplet spin state[3a] but rather appears to be a consequence of the highly electron releasing Cy-PSiP ligand set that supports spin pairing. Given the strong donor ability of the silyl group, it comes as no surprise that for **2**, **3**, and **5** a triplet spin state, which also favors a *fac*-κ^3-(PSiP)Ru^{II} ligation, is higher in energy by more than 24 kcal mol^{-1}.[18b] The strong metal d_{x2-y2} character of the HOMO, together with a smaller metal d_{xz} component that is involved in some Ru−X π bonding, is not particularly well suited to accommodate an agostic interaction at the vacant axial coordination site, while the LUMO exhibits Ru−X π* character featuring a strong metal d_{xy} component (cf. Figure S5 in the SI). Hence, agostic C−H interactions are not essential for stabilizing the singlet ground state. The rather weak C−H agostic interaction in **5**, which is estimated for (Cy-PSiP)RuNH(2-MeC_6H_4) (**5***) to amount to 2.3 kcal mol^{-1}, confirms this aspect.[18b]

In an attempt to put these findings into a broader perspective, analogues of **2**, **3**, and **5** that have the silyl group replaced by either C(sp^3)−Me (**2c**−**5c**), phosphido (**2p**−**5p**), or amido (**2n**−**5n**) donor groups were also studied computationally. According to the above rationale, key features of the modified compounds are expected to correlate with the electron-donating ability of the pincer's central donor. In agreement with chemical reasoning, the assessed NBO charge distribution reveals the following order of descending donating ability:[18b] PSiP > PPP > PCP > PNP. With regard to the strength of the C−H agostic interaction in **5***, DFT shows that it directly correlates with the degree of electron deficiency at Ru and hence increases in the following order (given in kcal mol^{-1}): **5*** (2.3) < **5*p** (3.8) < **5*c** (4.4) < **5*n** (7.3). The nature of the central donor group also has a profound influence on the gap in stability between *fac*-κ^3- and *mer*-κ^3-(Cy-PXP)Ru^{II} forms, which follows a regular trend as exemplified for complex **5** (given in kcal mol^{-1}): **5** (32.0) > **5p** (25.3) > **5c** (17.5) > **5n** (10.8). Of particular importance is the marked dependency revealed by DFT between the charge density at Ru and the size of the gap between the singlet and triplet spin states. The Δ*E*(S−T) gap decreases regularly for the silylamido complex from 24.2 (**3**) to 23.6 (**3p**), 22.7 (**3c**), and to 20.5 kcal mol^{-1} (**3n**), thereby reinforcing the pivotal role of a strongly donating central donor group for the stabilization of the singlet state of the four-coordinate 14-electron Ru^{II} complexes reported herein.

To acquire a more detailed view of the E−H bond activation steps involved in the formation of (Cy-PSiP)-supported

Scheme 3. Plausible Paths for E−H (E = B, N) Bond Activation of Ammonia-Borane (AB) by a Four-Coordinate, Formally 14-Electron (R-PSiP)RuX Complex (X = N(SiMe$_3$)$_2$)

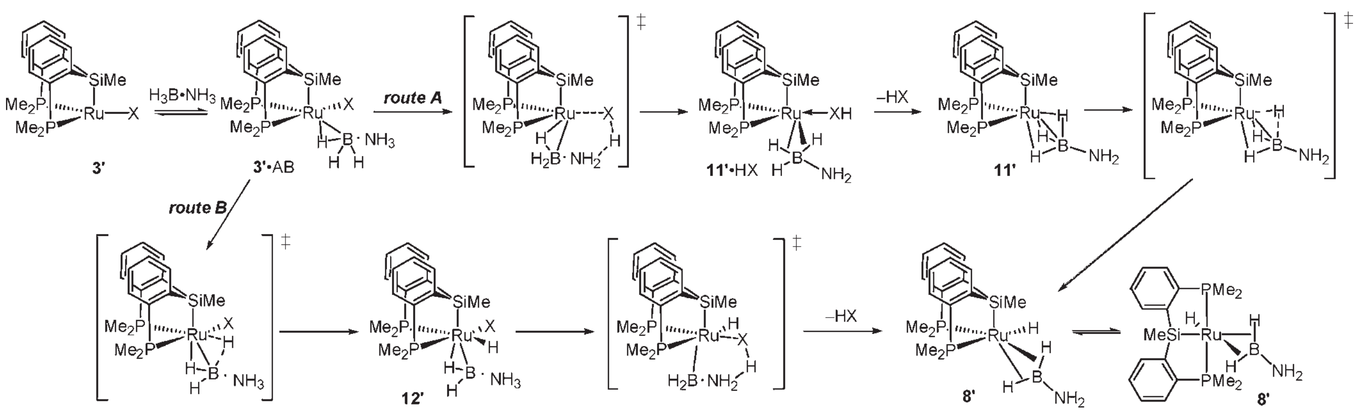

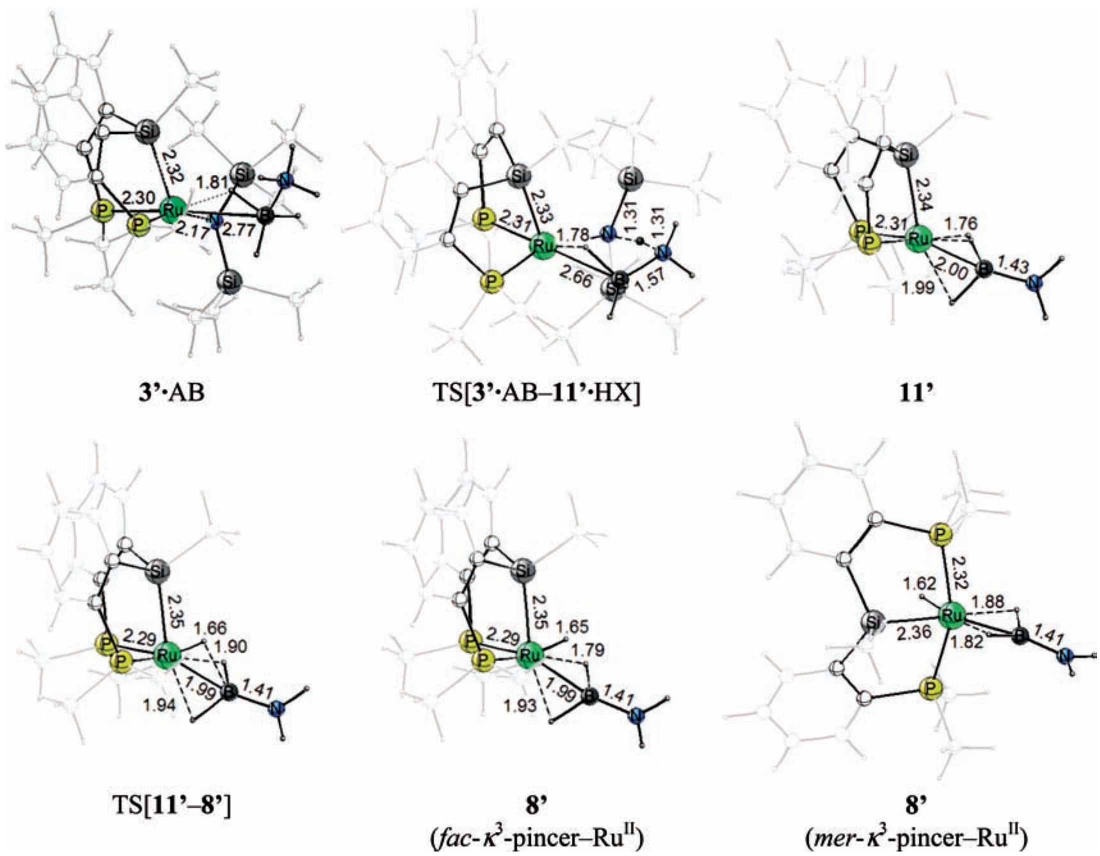

Figure 8. Selected metric parameters (Å) of the optimized structures of key stationary points for consecutive N−H and B−H bond activation of ammonia-borane (AB) by the four-coordinate (Me-PSiP)RuN(SiMe$_3$)$_2$ complex **3′** (cf. route A in Scheme 3).

bis(σ-B−H) aminoborane Ru complexes, two plausible routes have been explored computationally for the reaction of (Me-PSiP)RuN(SiMe$_3$)$_2$ (**3′**), in which the PCy$_2$ donor groups have been replaced by PMe$_2$, with H$_3$B·NH$_3$ (Scheme 3). One pathway (route A) entails an initial N−H bond activation of ammonia-borane (AB) in **3′**·AB to cleave the Ru−X bond protonolytically, thereby giving rise to adduct **11′**·HX. This intermediate is likely to release HX to furnish **11′**, which subsequently undergoes oxidative addition of the borane at the Ru^{II} center to generate the bis(σ-B−H) aminoborane complex **8′**. Oxidative addition of a B−H bond commencing from **3′**·AB, followed by Ru−X bond protonolysis via ammonia N−H bond activation, represents an alternate route B (Scheme 3).

The four-coordinate (Me-PSiP)RuN(SiMe$_3$)$_2$ compound **3′** readily binds H$_3$B·NH$_3$ to form the adduct **3′**·AB that features a weakly associated AB unit (d(Ru−N) = 2.772 Å) bound in an η^2-B−H fashion (Figure 8). Wiberg bond indices in **3′** support this view (Figure 9). Ammonia-borane association at the Ru^{II} center does not involve a significant barrier[19a] and is found to be somewhat uphill at the ΔH surface (ΔH = 2.7 kcal mol^{-1} relative

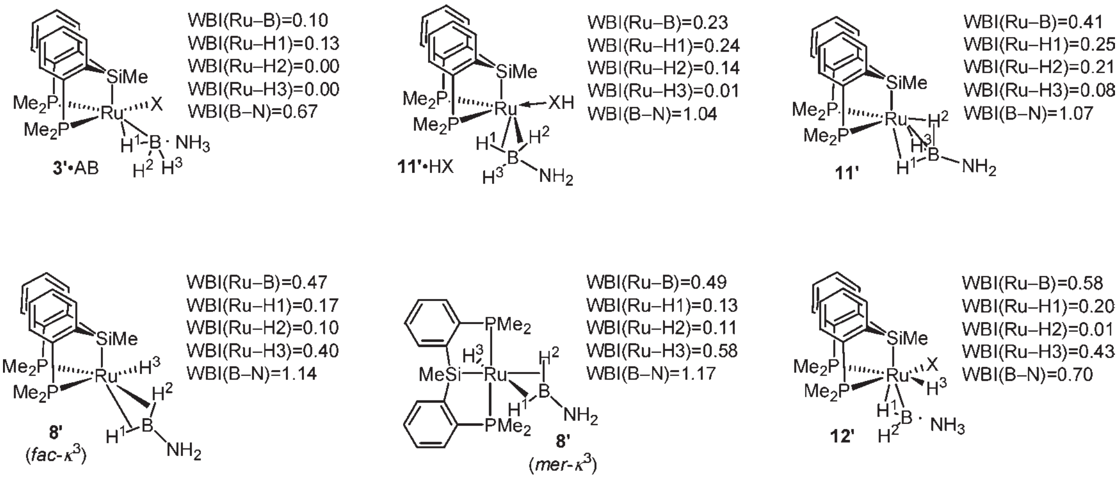

Figure 9. Wiberg bond indices for Ru and B centers in the compounds shown in Scheme 3 (X = $N(SiMe_3)_2$).

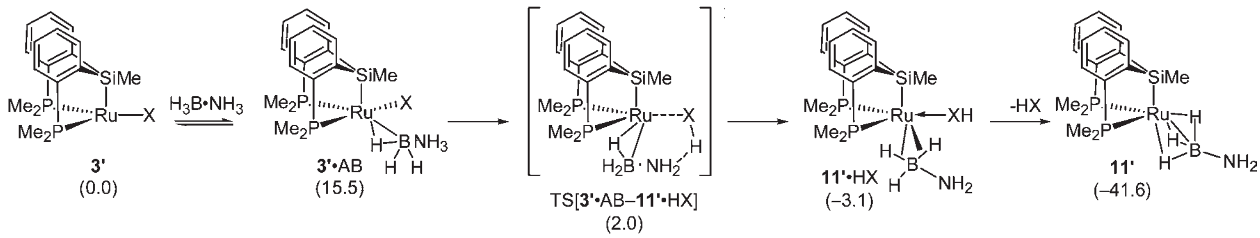

Figure 10. Free energies (kcal mol^{-1}) associated with the most accessible pathway for protonolytic Ru^{II}—N(amido) bond cleavage by ammonia-borane N—H activation in $3'\cdot$AB (X = $N(SiMe_3)_2$).[19b]

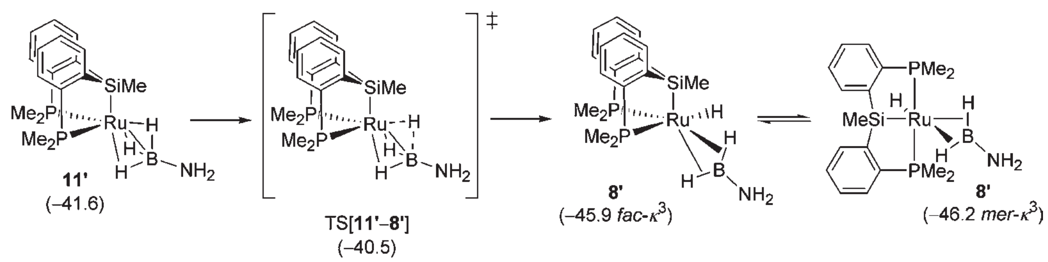

Figure 11. Free energies (kcal mol^{-1}) associated with the most accessible pathway for B—H oxidative addition of the H_3B—NH_2 fragment in **11′**.[19b]

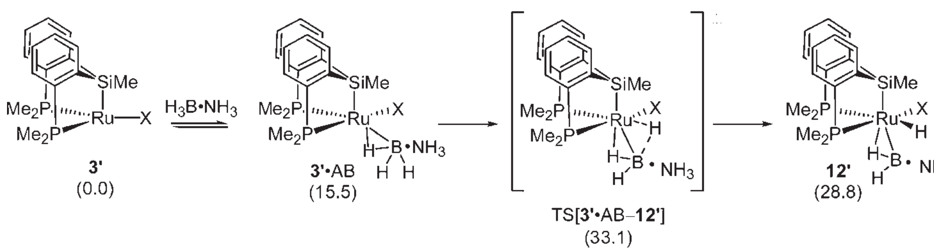

Figure 12. Free energies (kcal mol^{-1}) associated with the most accessible pathway for B—H oxidative addition of ammonia-borane in $3'\cdot$AB (with X = $N(SiMe_3)_2$).[19b]

to {3′ + AB}) and even more so when free energies are considered (Figure 10).

Focusing on route A (Figure 10), protonolytic Ru—N(amido) bond cleavage via N—H bond activation proceeds while traversing a metathesis-type transition state (TS) structure TS[$3'\cdot$AB—$11'\cdot$HX] featuring the concomitant N(ammonia)—H bond rupture and N(amido)—H bond formation together with strengthened/weakened B(borane)—N(ammonia) and Ru—N(amido) bonds, respectively. Because the increase in strength for several bonds overcompensates for partially attenuated bonds in TS[$3' \cdot$AB−$11' \cdot$HX], it comes as no surprise that the TS is low in free energy and only 2.0 kcal mol^{-1} above {$3'$ + AB}. The initially formed intermediate **11′**·HX is stabilized thereafter through $HN(SiMe_3)_2$ release. The kinetically facile ammonia-borane N−H activation is moreover driven by a thermodynamic force of substantial magnitude (ΔG = 41.6 kcal mol^{-1}) and can thus be expected to furnish **11′** instantaneously in an irreversible fashion (Figure 10).

Given the substantial energy gap between **11′**·HX and **11′**, borane oxidative addition at the Ru^{II} center preferably proceeds from **11′**, whereas a pathway commencing from **11′**·HX via key structures having the $HN(SiMe_3)_2$ molecule weakly associated is found to be less favorable. Borane B−H bond oxidative addition is moderately exergonic and has a rather small activation barrier to overcome in the process of traversing TS[**11′**−**8′**] (Figure 11). Although all the key species involved along the most accessible pathway for consecutive N−H and B−H bond activation adopt a *fac*-κ^3-(Me-PSiP)Ru^{II} ligation, *fac*-κ^3 and *mer*-κ^3 forms of **8′** are energetically close, with the latter being somewhat more stable.

The alternate route that initiates through borane oxidative addition to the Ru^{II} center in **3′**·AB has a prohibitively high barrier of 33.1 kcal mol^{-1} to overcome (Figure 12) and is thus at odds with the observed smooth activation of ammonia-borane by **3**. Our computational examination thus uncovered that ammonia-borane activation by (R-PSiP)RuX complexes likely proceeds in a stepwise fashion via ammonia N−H activation and subsequent borane B−H bond oxidative addition steps (route A in Scheme 3). The assessed moderate activation barriers together with the strong driving force for the overall transformation are consonant with the observed multiple, facile E−H bond activation steps. Notably, we were unable to locate a TS structure for N−H and B−H activation taking place simultaneously, suggesting that a concerted pathway of this type is not favorable in this system.[20]

■ SUMMARY AND CONCLUSIONS

In summary, unprecedented diamagnetic, four-coordinate, formally 14-electron (Cy-PSiP)RuX (X = amido, alkoxo) complexes that do not require agostic stabilization and that adopt a highly unusual trigonal pyramidal coordination geometry have been prepared and characterized by use of NMR spectroscopic, X-ray crystallographic, and DFT methods. Computational studies confirm the key role of the strongly σ-donating silyl group of the Cy-PSiP ligand in enforcing the unusual trigonal pyramidal coordination geometry. Unlike previously reported square planar examples of four-coordinate Ru^{II} complexes, the stability of the diamagnetic, four-coordinate, (Cy-PSiP)RuX complexes reported herein cannot be attributed to a triplet spin state but rather appears to be a consequence of the highly electron releasing Cy-PSiP ligand set. These results substantiate a new strategy for the synthesis of low-coordinate Ru species, whereby the use of a strongly σ-donating silyl ligand set helps to enforce coordinative unsaturation at the metal center.

Whereas silyl ligation serves to afford stability to the unusual trigonal pyramidal (Cy-PSiP)RuX complexes featured herein, these low-coordinate species are still capable of reacting with substrate E−H bonds. In exploring the reactivity of **2** and **3** as representative examples of trigonal pyramidal (Cy-PSiP)RuX species, we have found that these serve as precursors for the synthesis of a Ru dinuclear hydroxo complex as well as an η^5-oxocyclohexadienyl complex. Complexes **2** and **3** also undergo N−H/B−H bond activation reactions upon treatment with amine-borane reagents, including ammonia-borane, to form unusual bis(σ-B−H) complexes of the type (Cy-PSiP)RuH-(η^2:η^2-H_2BNRR') (R, R′ = H, alkyl). The mechanism of the activation of ammonia-borane by such low-coordinate (R-PSiP)RuX species was studied computationally and was determined to proceed most favorably in a stepwise fashion via intramolecular deprotonation of ammonia and subsequent borane B−H bond oxidative addition. These studies confirm that such four-coordinate, formally 14-electron (R-PSiP)RuX complexes are capable of promoting multiple bond activation steps in a manner that may be synthetically useful in the transformation of main group substrates. Work is currently underway to exploit this reactivity in substrate activation and functionalization.

■ EXPERIMENTAL SECTION

Experimental Details. All experiments were conducted under argon in an MBraun glovebox or using standard Schlenk techniques. Dry, oxygen-free solvents were used unless otherwise indicated. All nondeuterated solvents were deoxygenated and dried by sparging with nitrogen and subsequent passage through a double-column solvent purification system purchased from MBraun Inc. Tetrahydrofuran and diethyl ether were purified over two activated alumina columns, while benzene, toluene, and pentane were purified over one activated alumina column and one column packed with activated Q-5. All purified solvents were sparged with argon prior to use and stored over 4 Å molecular sieves. Benzene-d_6 and toluene-d_8 were degassed via three freeze−pump−thaw cycles and stored over 4 Å molecular sieves. The compound [(*p*-cymene)$RuCl_2$]$_2$ was purchased from Strem and used as received. The compound (2-$Cy_2PC_6H_4$)$_2$SiMeH was prepared according to literature procedures.[6b] Triethylamine was distilled from CaH_2. Water was degassed by sparging with argon. All other reagents were purchased from Aldrich and used without further purification. Unless otherwise stated, ^{1}H, ^{13}C, ^{31}P, ^{15}N, ^{11}B, and ^{29}Si NMR characterization data were collected at 300 K on a Bruker AV-500 spectrometer operating at 500.1, 125.8, 202.5, 50.7, 160.5, and 99.4 MHz (respectively) with chemical shifts reported in parts per million downfield of $SiMe_4$ (for ^{1}H, ^{13}C, and ^{29}Si), $MeNO_2$ (for ^{15}N), BF_3•OEt_2 (for ^{11}B), and 85% H_3PO_4 in D_2O (for ^{31}P). ^{1}H and ^{13}C NMR chemical shift assignments are based on data obtained from ^{13}C-DEPTQ, ^{1}H−^{1}H COSY, ^{1}H−^{13}C HSQC, and ^{1}H−^{13}C HMBC NMR experiments. ^{29}Si NMR assignments are based on ^{1}H−^{29}Si HMBC experiments. ^{15}N NMR assignments are based on ^{1}H−^{15}N HMQC experiments. In some cases, fewer than expected unique ^{13}C NMR resonances were observed, despite prolonged acquisition times. Elemental analyses were performed by Canadian Microanalytical Service Ltd. of Delta, British Columbia, Canada, Columbia Analytical Services of Tucson, Arizona, and Midwest Micro-Lab of Indianapolis, Indiana. Infrared spectra were recorded using a Bruker VECTOR 22 FT-IR spectrometer at a resolution of 4 cm^{-1}.

Computational Details. All calculations based on Kohn−Sham density functional theory (DFT)[21] were performed by means of the program package TURBOMOLE[22] using the almost nonempirical meta-GGA Tao−Perdue−Staroverov−Scuseria (TPSS) functional[23] within the RI-J integral approximation[24] in conjunction with flexible basis sets of triple-ζ quality. For ruthenium we used the Stuttgart−Dresden scalar-relativistic effective core potential (SDD, 28 core electrons)[25] in combination with the (7s7p5d1f)/[6s4p3d1f] (def2-TZVP) valence basis set.[26] All remaining elements were represented by Ahlrich's valence triple-ζ TZVP basis set[27] with polarization functions on all atoms. The good to excellent performance of the TPSS functional for a wide range of applications, with transition-metal complexes in particular, has been demonstrated previously.[28] To probe the influence of the DFT Hamiltonian on the singlet−triplet energy gap the hybrid meta-GGA TPSSh functional (i.e., TPSS with 10% exchange),[23,28a,29] which was reported to adequately describe spin-state energetics for transition metal complexes,[30] was also employed. The two DFT methods were shown to be equally capable of adequately describing spin-state energetics for the herein studied four-coordinate, 14-electron Ru^{II} complexes. Further details can be found in the Supporting Information. Analytical frequency calculations were performed to confirm that the reported transition states possess exactly one negative Hessian eigenvalue, while all other stationary points exhibit exclusively positive eigenvalues. The reaction and activation enthalpies and free energies (ΔH, $\Delta H^{\ddagger}$ and ΔG, $\Delta G^{\ddagger}$ at 298 K and 1 atm) were evaluated according to standard textbook procedures[31] using computed harmonic frequencies. Enthalpies were reported as ΔE + zero point energy corrections at 0 K + thermal motion corrections at 298 K and Gibbs free energies were obtained as $\Delta G = \Delta H - T\Delta S$ at 298 K. The analysis of the bonding situation was performed with the aid of Wiberg bond orders (WBO)[32] that are known to provide a good measure of the covalent bond order between two interacting atoms. Natural population analyses (NPA)[33] were performed with the NBO[34] in conjunction with the MAG-ReSpect[35] module. Optimized structures were visualized by employing the StrukEd program,[36] which was also used for the preparation of 3D molecule drawings.

[(Cy-PSiP)RuCl]$_2$ (1). A solution of (2-$Cy_2PC_6H_4)_2$SiMeH (1.4 g, 2.4 mmol) in ca. 5 mL of THF was added to a slurry containing [(*p*-cymene)$RuCl_2]_2$ (0.73 g, 1.2 mmol) and PCy_3 (0.67 g, 2.4 mmol) in ca. 10 mL of THF at room temperature. Neat Et_3N (0.33 mL, 2.4 mmol) was added to the reaction mixture via syringe. The resulting orange solution was heated to 70 °C with stirring for a period of 24 h. The THF solvent was removed in vacuo, and the resulting residue was triturated with pentane (3 × 1 mL). The remaining solid was washed with ca. 150 mL of benzene. The benzene washes were combined and filtered through a medium porosity glass frit. The filtrate was collected, and the volatile components were subsequently removed in vacuo. The remaining orange residue was washed with cold pentane (3 × 2 mL) and dried in vacuo to yield spectroscopically pure **1** (1.3 g, 74%) as an orange solid. ^1H NMR (333 K, 500 MHz, benzene-d_6): δ 7.82 (d, 2 H, H_{arom}, J = 7 Hz), 7.31 (m, 2 H, H_{arom}), 7.09 (t, 2 H, H_{arom}, J = 7 Hz), 6.93 (t, 2 H, H_{arom}, J = 7 Hz), 2.68 (br m, 2 H, P*Cy*), 2.61 − 2.45 (br overlapping resonances, 4 H, P*Cy*), 2.23−0.64 (br overlapping resonances, 41 H P*Cy* + Si*Me*; a singlet resonance at 1.56 ppm was assigned to the Si*Me* protons by use of a $^1H-^{13}C$ HSQC experiment). $^{13}C\{^1H\}$ NMR (333 K, 125.8 MHz, benzene-d_6): δ 159.5 (m, C_{arom}), 147.3 (br, C_{arom}), 132.0−131.8 (overlapping resonances, CH_{arom}), 129.9 (CH_{arom}), 126.2 (CH_{arom}), 41.5 (br m, CH_{Cy}), 37.6 (br m, CH_{Cy}), 31.1 (CH_{2Cy}), 30.1 (CH_{2Cy}), 29.0−28.4 (overlapping resonances, CH_{2Cy}), 27.3 (CH_{2Cy}), 27.1 (CH_{2Cy}), 2.6 (Si*Me*). $^{31}P\{^1H\}$ NMR (300 K, 202.5 MHz, benzene-d_6): δ 89.1. ^{29}Si NMR (300 K, 99.4 MHz, benzene-d_6): δ 65.2. Anal. Calcd for $C_{74}H_{110}P_4Si_2Ru_2Cl_2$: C, 61.18; H, 7.63. Found: C, 61.12; H, 7.57. A single crystal of **1**·3.5C_6H_6 suitable for X-ray diffraction analysis was grown by vapor diffusion of pentane into a benzene solution of **1**.

(Cy-PSiP)RuO^{t}Bu (2). A slurry of KO^{t}Bu (0.023 g, 0.21 mmol) in ca. 1 mL of benzene was added to a slurry of **1** (0.15 g, 0.10 mmol) in ca. 3 mL of benzene at room temperature. The reaction mixture was stirred for 1 h at room temperature over which time a color change from orange to red was observed. The solution was then filtered through Celite, and the filtrate was retained. The volatile components of the filtrate solution were removed in vacuo, and the resulting residue was triturated with pentane (2 × 1 mL) to yield **2** (0.15 g, 97%) as a red solid. ^1H NMR (500 MHz, benzene-d_6): δ 7.88 (d, 2 H, H_{arom}, J = 7 Hz), 7.44 (m, 2 H, H_{arom}), 7.14 (m, 2 H, H_{arom}), 7.01 (t, 2 H, H_{arom}, J = 7 Hz), 2.52 (br s, 2 H, P*Cy*), 2.32 (m, 2 H, P*Cy*), 2.18 (m, 2 H, P*Cy*), 2.04 (br m, 4 H, P*Cy*), 1.95 (m, 2 H, P*Cy*), 1.74−1.15 (overlapping resonances, 40 H, P*Cy* + O^t*Bu* + Si*Me*; singlet resonances at 1.50 and 1.33 ppm were assigned to the O^t*Bu* and Si*Me* protons, respectively, by use of a $^1H-^{13}C$ HSQC experiment), 1.04 (br m, 2 H, P*Cy*), 0.62 (br s, 2 H, P*Cy*). $^{13}C\{^1H\}$ NMR (125.8 MHz, benzene-d_6): δ 160.6 (d, C_{arom}, J_{CP} = 42 Hz), 148.0 (d, C_{arom}, J_{CP} = 48 Hz), 131.7 (d, CH_{arom}, J = 20 Hz), 129.1 (CH_{arom}), 127.0 (d, CH_{arom}, J = 5 Hz), 126.4 (CH_{arom}), 75.1 (OCMe$_3$), 40.2 (d, CH_{Cy}, J = 17 Hz), 37.4 (d, CH_{Cy}, J = 27 Hz), 35.5 (OC*Me*$_3$), 30.9 (CH_{2Cy}), 29.2−27.7 (overlapping resonances, CH_{2Cy}), 27.1 (CH_{2Cy}), 26.8 (CH_{2Cy}), 4.9 (Si*Me*). $^{31}P\{^1H\}$ NMR (202.5 MHz, benzene-d_6): δ 110.5. ^{29}Si NMR (99.4 MHz, benzene-d_6): δ 65.5. Anal. Calcd for $C_{41}H_{64}P_2OSiRu$: C, 64.43; H, 8.44. Found: C, 64.34; H, 8.33. A single crystal of **2**·C_6H_6·0.5C_5H_{12} suitable for X-ray diffraction analysis was grown by vapor diffusion of pentane into a benzene solution of **2**.

(Cy-PSiP)RuN(SiMe$_3$)$_2$ (3). A slurry of NaN(SiMe$_3$)$_2$ (0.027 g, 0.14 mmol) in ca. 1 mL of benzene was added to a slurry of **1** (0.10 g, 0.07 mmol) in ca. 3 mL of benzene at room temperature. The reaction mixture was stirred for 30 min at room temperature over which time a color change from orange to red was observed along with the formation of a white precipitate. The solution was then filtered through Celite, and the filtrate was collected. The volatile components of the filtrate solution were removed in vacuo, to give **3** as a red solid (0.086 g, 70%). ^1H NMR (500 MHz, benzene-d_6): δ 7.78 (d, 2 H, H_{arom}, J = 7 Hz), 7.39 (m, 2 H, H_{arom}), 7.11 (apparent t, 2 H, H_{arom}, J = 6 Hz), 6.99 (apparent t, 2 H, H_{arom}, J = 7 Hz), 2.33 (m, 2 H, P*Cy*), 2.15 (m, 2 H, P*Cy*), 2.06 (4 H, P*Cy*), 1.91−0.96 (broad overlapping resonances, 39 H, P*Cy* + Si*Me*; a singlet resonance at 1.33 ppm was assigned to the Si*Me* protons by use of a $^1H-^{13}C$ HSQC experiment), 0.65 (s, 9 H, NSi*Me*$_3$), 0.36 (s, 9 H, NSi*Me*$_3$). $^{13}C\{^1H\}$ NMR (125.8 MHz, benzene-d_6): δ 160.8 (d, C_{arom}, J = 41 Hz), 147.0 (d, C_{arom}, J = 48 Hz), 131.6 (d, CH_{arom}, J = 19 Hz), 129.2 (CH_{arom}), 127.2 (d, CH_{arom}, J = 4 Hz), 126.2 (CH_{arom}), 41.7 (d, CH_{Cy}, J = 17 Hz), 38.0 (d, CH_{Cy}, J = 27 Hz), 31.2 (CH_{2Cy}), 29.9 (CH_{2Cy}), 29.3−27.7 (overlapping resonances, CH_{2Cy}), 27.1 (CH_{2Cy}), 26.7 (CH_{2Cy}), 8.8 (NSi*Me*$_3$), 8.3 (NSi*Me*$_3$), 5.0 (Si*Me*). $^{31}P\{^1H\}$ NMR (202.5 MHz, benzene-d_6): δ 98.9. ^{29}Si NMR (99.4 MHz, benzene-d_6): δ 56.4 (P*Si*P), −6.2 (N*Si*Me$_3$). Anal. Calcd for $C_{43}H_{73}P_2NSi_3Ru$: C, 60.67; H, 8.64; N, 1.64. Found: C, 60.59; H, 8.36; N, 1.41. A single crystal of **3** suitable for X-ray diffraction analysis was grown from a concentrated diethyl ether solution at −30 °C.

(Cy-PSiP)RuNHPh (4). A solution of LiNHPh (0.015 g, 0.015 mmol) in ca. 1 mL of Et_2O was added to a slurry of **1** (0.11 g, 0.08 mmol) in ca. 5 mL of Et_2O at room temperature. The reaction mixture was stirred for 1 h at room temperature over which time a color change from orange to dark red was observed. The volatile components of the reaction mixture were removed in vacuo, and the remaining residue was washed with ca. 5 mL of benzene. The benzene solution was then filtered through Celite, and the filtrate solution was retained. The volatile components of the filtrate solution were removed in vacuo. The resulting dark red residue was triturated with pentane (3 × 2 mL) to yield **4** (0.11 g, 92%) as a dark red solid. ^1H NMR (500 MHz, benzene-d_6): δ 7.81 (d, 2 H, H_{arom}, J = 7 Hz), 7.46 (m, 2 H, H_{arom}), 7.19−7.13 (overlapping resonances, 4 H, H_{arom} + NHPh_{meta}), 7.02 (t, 2 H, H_{arom}, J = 7 Hz), 6.93 (d, 2 H, NHPh_{ortho}, J = 8 Hz), 6.70 (t, 1 H, NHPh_{para}, J = 7 Hz), 6.35 (br s, 1 H, N*H*Ph), 2.54 (m, 2 H, P*Cy*), 2.29−2.08 (overlapping resonances, 6 H, P*Cy*), 1.91−1.06 (overlapping resonances, 34 H, P*Cy*), 1.00 (s, 3 H, Si*Me*), 0.71 (br s, 2 H, P*Cy*). $^{13}C\{^1H\}$ NMR (125.8 MHz, benzene-d_6): δ 159.3 (d, C_{arom}, J = 40 Hz), 157.3 (NH*Ph*, C_{ipso}), 147.5 (d, C_{arom}, J = 47 Hz), 131.7 (d, CH_{arom}, J = 19 Hz), 130.2 (CH_{arom}), 128.9 (NH*Ph*, C_{meta}), 127.2 (d, CH_{arom}, J = 4 Hz), 126.7 (CH_{arom}), 117.7 (NH*Ph*, C_{para}), 117.4 (NH*Ph*, C_{ortho}), 40.5 (d, CH_{Cy}, J = 14 Hz), 38.4 (d, CH_{Cy}, J = 28 Hz), 33.1 (CH_{2Cy}), 30.6 (CH_{2Cy}), 29.9 (CH_{2Cy}), 29.3 (CH_{2Cy}), 29.2 (CH_{2Cy}), 28.5−27.8 (overlapping resonances, CH_{2Cy}), 27.1 (CH_{2Cy}), 26.8 (CH_{2Cy}), −0.02 (Si*Me*). $^{31}P\{^1H\}$ NMR (202.5 MHz, benzene-d_6): δ 96.5. ^{29}Si NMR (99.4 MHz, benzene-d_6): δ 58.7. ^{15}N NMR (50.7 MHz, benzene-d_6): δ −220.5. Anal. Calcd for $C_{43}H_{61}P_2NSiRu$: C, 65.95; H, 7.85; N, 1.79. Found: C, 65.91; H, 7.48; N, 2.13.

(Cy-PSiP)RuNH(2,6-$Me_2C_6H_3$) (5). A slurry of LiNH(2,6-$Me_2C_6H_3$) (0.017 g, 0.14 mmol) in ca. 3 mL of benzene was added to a slurry of **1** (0.10 g, 0.07 mmol) in ca. 5 mL of benzene at room temperature. The reaction mixture was stirred for 1 h at room temperature over which time a color change from orange to dark red was observed along with the formation of a white precipitate. The solution was then filtered through Celite, and the filtrate solution was retained. The volatile components of the filtrate solution were removed in vacuo, and the resulting residue was triturated with pentane (ca. 1 mL) to yield **5** (0.11 g, 96%) as a dark red solid. ^{1}H NMR (500 MHz, benzene-d_6): δ 7.92 (d, 2 H, H_{arom}, J = 7 Hz), 7.57 (br s, 1 H, NH), 7.49 (m, 2 H, H_{arom}), 7.24−7.18 (overlapping resonances, 4 H, H_{arom} + 2,6-$Me_2C_6H_3$), 7.05 (t, 2 H, H_{arom}, J = 7 Hz), 6.86 (t, 1 H, 2,6-$Me_2C_6H_3$, J = 7 Hz), 2.52 (m, 2 H, PCy), 2.31 (s, 6 H, 2,6-$Me_2C_6H_3$), 2.21 (m, 2 H, PCy), 1.83 (m, 4 H, PCy), 1.65−0.70 (overlapping resonances, 37 H, PCy + SiMe; a singlet resonance at 1.25 ppm was assigned to the SiMe protons by use of a ^{1}H−^{13}C HSQC experiment), 0.62 (br m, 2 H, PCy). ^{13}C{^{1}H} NMR (125.8 MHz, benzene-d_6): δ 158.4 (C_{arom}), 158.3 ($Me_2C_6H_3$, C_{ipso}), 148.1 (C_{arom}), 131.2 (d, CH_{arom}, J = 19 Hz), 128.3 (CH_{arom}), 127.7 (2,6-$Me_2C_6H_3$, CH_{meta}), 126.6 (d, CH_{arom}, J = 5 Hz), 125.8 (CH_{arom}), 122.9 (NC_{ipso}), 116.2 (2,6-$Me_2C_6H_3$, CH_{para}), 39.7 (d, CH_{Cy}, J = 13 Hz), 38.0 (d, CH_{Cy}, J = 25 Hz), 32.9 (CH_{2Cy}), 29.7 (CH_{2Cy}), 28.6−26.8 (overlapping resonances, CH_{2Cy}), 26.5 (CH_{2Cy}), 26.1 (CH_{2Cy}), 18.8 ($Me_2C_6H_3$), −1.7 (SiMe). ^{31}P{^{1}H} NMR (202.5 MHz, benzene-d_6): δ 94.2. ^{29}Si NMR (99.4 MHz, benzene-d_6): δ 57.2. ^{15}N NMR (50.7 MHz, benzene-d_6): δ −219.1. Anal. Calcd for $C_{45}H_{65}P_2NSiRu$: C, 66.63; H, 8.13; N, 1.76. Found: C, 66.50; H, 7.81; N, 1.68. A single crystal of **5** suitable for X-ray diffraction analysis was grown from a concentrated diethyl ether solution at −30 °C.

[(Cy-PSiP)RuOH]$_2$ (6). A solution of **2** (0.21 g, 0.28 mmol) in ca. 3 mL of benzene was treated with degassed H_2O (0.005 mL, 0.28 mmol). An immediate color change from red to orange was observed. The volatile components of the reaction mixture were removed in vacuo, and the solid was triturated with pentane (2 × 1 mL) to yield **6** (0.19 g, 94%) as an orange solid. ^{1}H NMR (500 MHz, benzene-d_6): δ 8.02 (br s, 1 H, H_{arom}), 7.72 (br s, 1 H, H_{arom}), 7.72 (br s, 1 H, H_{arom}), 7.51 (br s, 1 H, H_{arom}), 7.24 (br s, 2 H, H_{arom}), 7.04 (br s, 2 H, H_{arom}), 6.94 (br s, 1 H, H_{arom}), 3.22 (br s, 1 H, PCy), 3.03 (br s, 1 H, PCy), 2.79 (br s, 1 H, PCy), 2.64 (br s, 1 H, PCy), 2.51 (br s, 1 H, PCy), 2.42 (br s, 1 H, PCy), 2.24 (m, 2 H, PCy), 2.09−0.80 (overlapping resonances, 34 H, PCy + SiMe; a singlet resonance at 1.52 ppm was assigned to the SiMe protons by use of a ^{1}H−^{13}C HSQC experiment), 0.65 (br m, 2 H, PCy), 0.37 (br s, 1 H, PCy), −0.13 (br s, 1 H, PCy), −0.37 (br s, 1 H, PCy), −0.74 (s, 1 H, OH). ^{13}C{^{1}H} NMR (125.8 MHz, benzene-d_6): δ 160.4 (br, C_{arom}), 132.7 (m, CH_{arom}), 131.1 (m, CH_{arom}), 129.2 (CH_{arom}), 128.9 (CH_{arom}), 127.8 (CH_{arom}), 126.4 (CH_{arom}), 126.3 (CH_{arom}), 41.3 (m, CH_{Cy}), 39.9 (m, CH_{Cy}), 36.1 (m, CH_{Cy}), 34.8−26.7 (br overlapping resonances, CH_{2Cy}), 3.7 (SiMe). ^{31}P{^{1}H} NMR (300 K, 202.5 MHz, benzene-d_6): δ 91.2 (d, 2 P, $^2J_{PP}$ = 25 Hz), 86.5 (d, 2 P, $^2J_{PP}$ = 25 Hz). ^{31}P{^{1}H} NMR (363 K, 202.5 MHz, toluene-d_8): δ 94.8 (br s). ^{29}Si NMR (99.4 MHz, benzene-d_6): δ 68.7. Anal. Calcd for $C_{74}H_{112}P_4O_2Si_2Ru_2$: C, 62.77; H, 7.97. Found: C, 62.34; H, 8.15. A single crystal of **6**·C_7H_8 suitable for X-ray diffraction analysis was grown from a concentrated toluene solution.

(Cy-PSiP)Ru(η^5-C_6H_5O) (7). A solution of **2** (0.16 g, 0.21 mmol) in ca. 3 mL of benzene was treated with a solution of HOPh (0.020 g, 0.21 mmol) in ca. 1 mL of benzene at room temperature resulting in a color change from red to pale yellow. The volatile components of the reaction mixture were removed in vacuo, and the resulting residue was washed with pentane (3 × 1 mL) to yield **7** (0.14 g, 84%) as a white solid. ^{1}H NMR (500 MHz, benzene-d_6): δ 7.63 (br m, 2 H, H_{arom}), 7.27 (br s, 2 H, H_{arom}), 7.08 (br m, 2 H, H_{arom}), 6.97 (br m, 2 H, H_{arom}), 5.62 (br m, 2 H, Ru-η^5-C_6H_5O), 5.14 (br d, 2 H, Ru-η^5-C_6H_5O, J = 5 Hz), 3.98 (apparent t, 1 H, Ru-η^5-C_6H_5O, J = 5 Hz), 2.46 (br m, 4 H, PCy), 1.92 (br s, 2 H, PCy), 1.85−0.93 (br overlapping resonances, 37 H, PCy), 0.89 (s, 3 H, SiMe), 0.62 (br s, 2 H, PCy). ^{13}C{^{1}H} NMR (125.8 MHz, benzene-d_6): δ 169.9 (Ru-η^5-C_6H_5O), 158.7 (d, C_{arom}, J = 44 Hz), 147.2 (d, C_{arom}, J = 45 Hz), 132.2 (d, CH_{arom}, J = 19 Hz), 129.8 (CH_{arom}), 129.0 (CH_{arom}), 126.9 (CH_{arom}), 99.1 (Ru-η^5-C_6H_5O), 83.3 (Ru-η^5-C_6H_5O), 67.6 (Ru-η^5-C_6H_5O), 41.4 (br, CH_{Cy}), 38.9 (br, CH_{Cy}), 32.4−25.9 (br, CH_{2Cy}), 2.7 (SiMe). ^{31}P{^{1}H} NMR (300 K, 202.5 MHz, benzene-d_6): δ 74.7 (br m). ^{31}P{^{1}H} NMR (363 K, 202.5 MHz, toluene-d_8): δ 71.5 (s). ^{31}P{^{1}H} NMR (213 K, 101.3 MHz, toluene-d_8): δ 87.7 (br s, 1 P, Cy-PSiP), 66.7 (br s, 1 P, Cy-PSiP). ^{29}Si NMR (99.4 MHz, benzene-d_6): δ 57.4. Anal. Calcd for $C_{43}H_{60}OP_2$-SiRu: C, 65.87; H, 7.71. Found: C, 65.85; H, 7.90. A single crystal of **7**·C_6H_6 suitable for X-ray diffraction analysis was grown from a concentrated benzene solution.

(Cy-PSiP)RuH(η^2:η^2-H_2BNH_2) (8). A solution of $H_3B\cdot NH_3$ (0.004 g, 0.12 mmol) in ca. 2 mL of benzene was added to a room-temperature solution of **2** (0.092 g, 0.12 mmol) in ca. 10 mL of benzene. An immediate color change from red to yellow was observed. The volatile components of the reaction mixture were removed in vacuo, and the remaining solid was triturated with hexanes (2 × 1 mL) to yield **8** (0.070 g, 81%) as a yellow solid. ^{1}H NMR (500 MHz, benzene-d_6): δ 8.25 (d, 2 H, H_{arom}, J = 7 Hz), 7.51 (m, 2 H, H_{arom}), 7.30 (t, 2 H, H_{arom}, J = 7 Hz), 7.20 (t, 2 H, H_{arom}, J = 7 Hz), 2.44 (br s, 2 H, NH_2), 2.36 (m, 4 H, PCy), 1.94−1.17 (overlapping resonances, 40 H, PCy), 0.99 (s, 3 H, SiMe), −3.36 (br s, 1 H, RuHB), −7.50 (br s, 1 H, RuHB), −12.62 (t, 1 H, RuH, $^2J_{HP}$ = 26 Hz). ^{13}C{^{1}H} NMR (125.8 MHz, benzene-d_6): δ 161.6 (apparent t, C_{arom}, J = 26 Hz), 146.1 (apparent t, C_{arom}, J = 24 Hz), 133.1 (apparent t, CH_{arom}, J = 10 Hz), 129.2 (CH_{arom}), 129.1 (CH_{arom}), 126.8 (CH_{arom}), 42.1 (apparent t, CH_{Cy}, J = 8 Hz), 35.5 (apparent t, CH_{Cy}, J = 13 Hz), 31.0 (CH_{2Cy}), 30.4 (CH_{2Cy}), 30.0 (CH_{2Cy}), 29.0 (CH_{2Cy}), 28.5−27.7 (overlapping resonances, CH_{2Cy}), 9.7 (SiMe). ^{31}P{^{1}H} NMR (202.5 MHz, benzene-d_6): δ 90.1. ^{29}Si NMR (99.4 MHz, benzene-d_6): δ 63.5. ^{11}B{^{1}H} NMR (160 MHz, benzene-d_6): δ 44.1 (br). ^{15}N NMR (50.7 MHz, benzene-d_6): δ −310.1. IR (Nujol, cm^{-1}): ν 3499, 3399 (s, N−$H_{s,as}$); 1964 (m br, Ru−H); 1818 (w br, Ru−H−B); 1588 (s, N−H_{bend}). Anal. Calcd for $C_{37}H_{60}P_2NBSiRu$: C, 61.65; H, 8.39; N, 1.94. Found: C, 61.31; H, 8.36; N, 1.69. A single crystal of **8** suitable for X-ray diffraction analysis was grown from a concentrated Et_2O solution at −35 °C.

(Cy-PSiP)RuH(η^2:η^2-H_2BNMe_2) (9). A solution of of **2** (0.074 g, 0.097 mmol) in ca. 5 mL of benzene was treated with a solution of $H_3B\cdot NHMe_2$ (0.006 g, 0.097 mmol) in ca. 2 mL of benzene at room temperature. An immediate color change from red to yellow was observed. The volatile components of the reaction mixture were removed in vacuo, and the remaining solid was washed with pentane (2 × 1 mL) to yield **9** (0.049 g, 67%) as a white solid. ^{1}H NMR (300 K, 500 MHz, benzene-d_6): δ 8.26 (d, 2 H, H_{arom}, J = 7 Hz), 7.53 (m, 2 H, H_{arom}), 7.31 (apparent t, 2 H, H_{arom}, J = 7 Hz), 7.20 (apparent t, 2 H, H_{arom}, J = 7 Hz), 2.59 (s, 6 H, NMe_2), 2.45−2.30 (overlapping resonances, 4 H, PCy), 1.96−1.04 (overlapping resonances, 40 H, PCy), 0.97 (s, 3 H, SiMe), −3.29 (br s, 1 H, H_2B), −7.49 (br s, 1 H, H_2B), −13.07 (t, 1 H, RuH, $^2J_{HP}$ = 25 Hz). ^{13}C{^{1}H} NMR (300 K, 125.8 MHz, benzene-d_6): δ 161.7 (apparent t, C_{arom}, J_{CP} = 26 Hz), 146.2 (apparent t, C_{arom}, J_{CP} = 24 Hz), 133.0 (apparent t, CH_{arom}, J = 10 Hz), 129.1 (CH_{arom}), 129.0 (CH_{arom}), 126.8 (CH_{arom}), 42.7 (apparent t, CH_{Cy}, J = 8 Hz), 40.9 (br s, NMe_2), 35.5 (apparent t, CH_{Cy}, J = 13 Hz), 31.3 (CH_{2Cy}), 30.4 (CH_{2Cy}), 30.1 (CH_{2Cy}), 29.1 (CH_{2Cy}), 28.4 (m, CH_{2Cy}), 28.1 (m, CH_{2Cy}), 27.9−27.7 (overlapping resonances, CH_{2Cy}), 27.2 (CH_{2Cy}), 10.5 (SiMe). ^{31}P{^{1}H} NMR (300 K, 202.5 MHz, benzene-d_6): δ 91.2. ^{29}Si NMR (300 K, 99.4 MHz, benzene-d_6): δ 63.7. ^{11}B NMR (300 K, 160 MHz, benzene-d_6): δ 43.9 (br). IR (thin film, cm^{-1}): ν 1966 (m br, Ru−H); the B−H stretches could not be unequivocally identified. Anal. Calcd for $C_{39}H_{64}P_2NBSiRu$: C, 62.55; H, 8.61; N, 1.87. Found: C, 62.34; H, 8.98; N, 1.68. A single crystal of **9** suitable for X-ray diffraction analysis was grown from a concentrated Et_2O solution at −35 °C.

(Cy-PSiP)RuH(η^2:η^2-H_2BNH^tBu) (10). A solution of **2** (0.075 g, 0.098 mmol) in ca. 5 mL of benzene was treated with a solution of $H_3B\cdot NH_2{}^tBu$ (0.009 g, 0.098 mmol) in ca. 2 mL of benzene at room temperature. An immediate color change from red to yellow was observed. The volatile components of the reaction mixture were removed in vacuo, and the remaining solid was washed with pentane (2 × 1 mL) to yield **10** (0.062 g, 82%) as a white solid. ^1H NMR (500 MHz, benzene-d_6): δ 8.26 (d, 2 H, H_{arom}, J = 7 Hz), 7.53 (m, 2 H, H_{arom}), 7.31 (apparent t, 2 H, H_{arom}, J = 7 Hz), 7.21 (apparent t, 2 H, H_{arom}, J = 7 Hz), 3.29 (br s, 1 H, N*H*), 2.33 (br m, 4 H, P*Cy*), 2.06−1.13 (overlapping resonances, 40 H, P*Cy*), 1.11 (s, 9 H, NC*Me*$_3$), 0.96 (s, 3 H, Si*Me*), −3.34 (br s, 1 H, Ru*H*B), −7.56 (br s, 1 H, Ru*H*B), −12.66 (br s, 1 H, Ru*H*). $^{13}C\{^1H\}$ NMR (125.8 MHz, benzene-d_6): δ 161.6 (apparent t, C_{arom}, J_{CP} = 25 Hz), 146.5 (apparent t, C_{arom}, J_{CP} = 23 Hz), 132.9 (apparent t, CH_{arom}, J = 10 Hz), 129.0 (CH_{arom}), 128.9 (CH_{arom}), 126.7 (CH_{arom}), 50.0 ($NCMe_3$), 42.8 (apparent t, CH_{Cy}, J = 8 Hz), 36.1 (br, CH_{Cy}), 32.4 (NC*Me*$_3$), 30.3 (CH_{2Cy}), 29.9 (CH_{2Cy}), 29.0 (CH_{2Cy}), 27.8 (CH_{2Cy}), 27.0 (CH_{2Cy}), 10.1 (Si*Me*). $^{31}P\{^1H\}$ NMR (202.5 MHz, benzene-d_6): δ 90.2. ^{29}Si NMR (99.4 MHz, benzene-d_6): δ 64.2. $^{11}B\{^1H\}$ NMR (160 MHz, benzene-d_6): δ 42.1 (br). IR (thin film, cm^{-1}): ν 3310 (br s, N−H); 1966 (m br, Ru−H); the B−H stretches could not be unequivocally identified. Anal. Calcd for $C_{41}H_{68}P_2NBSiRu$: C, 63.39; H, 8.82; N, 1.80. Found: C, 63.25; H, 8.80; N, 1.66.

■ ASSOCIATED CONTENT

Ⓢ Supporting Information. Crystallographic solution and refinement details for $\mathbf{1}\cdot 3.5C_6H_6$, $\mathbf{2}\cdot C_6H_6\cdot 0.5C_5H_{12}$, **3**, **5**, $\mathbf{6}\cdot C_7H_8$, $\mathbf{7}\cdot C_6H_6$, **8**, and **9**, including an ORTEP diagram of **9** as well as crystallographic data (CIF) and computational details. This material is available free of charge via the Internet at http://pubs.acs.org.

■ AUTHOR INFORMATION

Corresponding Author
st40@st-andrews.ac.uk; laura.turculet@dal.ca

■ ACKNOWLEDGMENT

We are grateful to the Natural Sciences and Engineering Research Council (NSERC) of Canada and Dalhousie University for their support of this work. We also thank Dr. M. Lumsden (NMR3, Dalhousie) for assistance in the acquisition of NMR data.

■ REFERENCES

(1) Hartwig, J. F. *Organotransition metal chemistry: from bonding to catalysis*; University of Science Books: Sausalito, CA, 2010.

(2) *Comprehensive Organometalic Chemistry III, Vol. 6: Compounds of Group 8*; Mingos, D. P. M., Crabtree, R. H., Bruce, M., Eds.; Elsevier Ltd.: Oxford, UK, 2007.

(3) (a) Watson, L. A.; Ozerov, O. V.; Pink, M.; Caulton, K. G. *J. Am. Chem. Soc.* **2003**, *125*, 8426. (b) Walstrom, A.; Pink, M.; Caulton, K. G. *Inorg. Chem.* **2006**, *45*, 5617. (c) Askevold, B.; Khusniyarov, M. M.; Herdtweck, E.; Meyer, K.; Schneider, S. *Angew. Chem., Int. Ed.* **2010**, *49*, 7566.

(4) A four-coordinate structure lacking agostic interactions has been proposed for $[(IMes)_2Ru(H)(CO)][BAr'_4]$ (IMes = 1,3-bis(2,4,6-trimethylphenyl)imidazol-2-ylidene, BAr'_4 = 3,5-$(CF_3)_2C_6H_3$), although this complex has not been crystallographically characterized: Lee, J. P.; Ke, Z.; Ramírez, M. A.; Gunnoe, T. B.; Cundari, T. R.; Boyle, P. D.; Petersen, J. L. *Organometallics* **2009**, *28*, 1758.

(5) (a) Huang, D.; Streib, W. E.; Bollinger, J. C.; Caulton, K. G.; Winter, R. F.; Scheiring, T. *J. Am. Chem. Soc.* **1999**, *121*, 8087. (b) Huang, D.; Huffman, J. C.; Streib, W. E.; Folting, K.; Young, V.; Eisenstein, O.; Caulton, K. G. *Organometallics* **2000**, *19*, 2281. (c) Huang, D.; Huffman, J. C.; Bollinger, J. C.; Eisenstein, O.; Caulton, K. G. *J. Am. Chem. Soc.* **1997**, *119*, 7398. (d) Baratta, W.; Herdtweck, E.; Rigo, P. *Angew. Chem., Int. Ed.* **1999**, *38*, 1629. (e) Vieille-Petit, L.; Luan, X.; Gatti, M.; Blumentritt, S.; Linden, A.; Clavier, H.; Nolan, S. P.; Dorta, R. *Chem. Commun.* **2009**, 3783.

(6) (a) MacInnis, M. C.; MacLean, D. F.; Lundgren, R. J.; McDonald, R.; Turculet, L. *Organometallics* **2007**, *26*, 6522. (b) MacLean, D. F.; McDonald, R.; Ferguson, M. J.; Caddell, A. J.; Turculet, L. *Chem. Commun.* **2008**, 5146. (c) Mitton, S. J.; McDonald, R.; Turculet, L. *Organometallics* **2009**, *28*, 5122. (d) Morgan, E.; MacLean, D. F.; McDonald, R.; Turculet, L. *J. Am. Chem. Soc.* **2009**, *131*, 14234. (e) Mitton, S. J.; McDonald, R.; Turculet, L. *Angew. Chem., Int. Ed.* **2009**, *48*, 8568.

(7) Johnson, T. D.; Folting, K.; Streib, W. E.; Martin, J. D.; Huffman, J. C.; Jackson, S. A.; Eisenstein, O.; Caulton, K. G. *Inorg. Chem.* **1995**, *34*, 488.

(8) Sanford, M. S.; Henling, L. M.; Day, M. W.; Grubbs, R. H. *Angew. Chem., Int. Ed.* **2000**, *39*, 3451.

(9) The four-coordinate phosphonium alkylidene complex $[(H_2IMes)Cl_2Ru{=}C(H)PCy_3][B(C_6F_5)_4]$ also exhibits distorted trigonal pyramidal coordination geometry in the solid state: Romero, P. E.; Piers, W. E.; McDonald, R. *Angew. Chem., Int. Ed.* **2004**, *43*, 6161.

(10) (a) Koelle, U. *Chem. Rev.* **1998**, *98*, 1313. (b) Loren, S. D.; Campion, B. K.; Heyn, R. H.; Tilley, T. D.; Bursten, B. E.; Luth, K. W. *J. Am. Chem. Soc.* **1989**, *111*, 4712.

(11) Blake, R. E., Jr.; Heyn, R. H.; Tilley, T. D. *Poyhedron* **1992**, *11*, 709.

(12) Cole-Hamilton, D. J.; Young, R. J.; Wilkinson, G. *J. Chem. Soc., Dalton Trans.* **1976**, 1995.

(13) Koelle, U.; Hörnig, A.; Englert, U. *Organometallics* **1994**, *13*, 4064.

(14) (a) Alcaraz, G.; Vendier, L.; Clot, E.; Sabo-Etienne, S. *Angew. Chem., Int. Ed.* **2010**, *49*, 918. (b) Alcaraz, G.; Sabo-Etienne, S. *Angew. Chem., Int. Ed.* **2010**, *49*, 7170. (c) Tang, C. Y.; Thompson, A. L.; Aldridge, S. *Angew. Chem., Int. Ed.* **2010**, *49*, 921. (d) Douglas, T. M.; Chaplin, A. B.; Weller, A. S. *J. Am. Chem. Soc.* **2008**, *130*, 14432. (e) Chaplin, A. B.; Weller, A. S. *Inorg. Chem.* **2010**, *49*, 1111. (f) Alcaraz, G.; Chaplin, A. B.; Stevens, C. J.; Clot, E.; Vendier, L.; Weller, A. S.; Sabo-Etienne, S. *Organometallics* **2010**, *29*, 5591. (g) Stevens, C. J.; Dallanegra, R.; Chaplin, A. B.; Weller, A. S.; Macgregor, S. A.; Ward, B.; McKay, D.; Alcaraz, G.; Sabo-Etienne, S. *Chem.—Eur. J.* **2011**, *17*, 3011.

(15) Klooster, W. T.; Koetzle, T. F.; Siegbahn, P. E. M.; Richardson, T. B.; Crabtree, R. H. *J. Am. Chem. Soc.* **1999**, *121*, 6337.

(16) (a) Staubitz, A.; Robertson, A. P. M.; Manners, I. *Chem. Rev.* **2010**, *110*, 4079. (b) Hamilton, C. W.; Baker, R. T.; Staubitz, A.; Manners, I. *Chem. Soc. Rev.* **2009**, *38*, 279. (c) Stephens, F. H.; Pons, V.; Baker, R. T. *Dalton Trans.* **2007**, 2613.

(17) For an example of catalytic dehydrogenation of ammonia borane by a Ru amido complex, see: Blaquiere, N.; Diallo-Garcia, S.; Gorelsky, S. I.; Black, D. A.; Fagnou, K. *J. Am. Chem. Soc.* **2008**, *130*, 14034.

(18) (a) Calculations employed TURBOMOLE V6.0 and used the almost nonempirical TPSS functional together with flexible basis sets of valence triple-ζ quality. (b) See the Supporting Information for full details.

(19) (a) Examination by a linear-transit approach gave no indication that this process is associated with a significant enthalpic barrier. (b) Free energies [kcal mol^{-1}] are given relative to $\{\mathbf{3'} + H_3B\cdot NH_3\}$.

(20) The ability of Ru amido species to extrude H_2 from secondary alcohols via concerted reaction pathways has been established: (a) Clapham, S. E.; Hadzovic, A.; Morris, R. H. *Coord. Chem. Rev.* **2004**, *248*, 2201. (b) Noyori, R.; Hashiguchi, S. *Acc. Chem. Res.* **1997**, *30*, 97.

(21) Parr, R. G.; Yang, W. *Density-Functional Theory of Atoms and Molecules*; Oxford University Press: New York, NY, 1989.

(22) (a) Ahlrichs, R.; Bär, M.; Häser, M.; Horn, H.; Kölmel, C. *Chem. Phys. Lett.* **1989**, *162*, 165. (b) Treutler, O.; Ahlrichs, R. *J. Chem. Phys.* **1995**, *102*, 346. (c) Ahlrichs, R.; Furche, F.; Hättig, C.; Klopper, W.; Sierka, M.; Weigend, F. *TURBOMOLE*, version 6.0; University of Karlsruhe: Karlsruhe, Germany, 2009; http://www.turbomole.com.

(23) (a) Dirac, P. A. M. *Proc. R. Soc. London* **1929**, *A123*, 714. (b) Slater, J. C. *Phys. Rev.* **1951**, *81*, 385. (c) Perdew, J. P.; Wang, Y. *Phys. Rev.* **1992**, *B45*, 13244. (d) Tao, J.; Perdew, J. P.; Staroverov, V. N.; Scuseria, G. E. *Phys. Rev. Lett.* **2003**, *91*, 146401. (e) Perdew, J. P.; Tao, J.; Staroverov, V. N.; Scuseria, G. E. *J. Chem. Phys.* **2004**, *120*, 6898.

(24) (a) Vahtras, O.; Almlöf, J.; Feyereisen, M. W. *Chem. Phys. Lett.* **1993**, *213*, 514. (b) Eichkorn, K.; Treutler, O.; Öhm, H.; Häser, M.; Ahlrichs, R. *Chem. Phys. Lett.* **1995**, *242*, 652.

(25) Andrae, D.; Häuβermann, U.; Dolg, M.; Stoll, H.; Preuß, H. *Theor. Chim. Acta* **1990**, *77*, 123.

(26) (a) Weigend, F.; Ahlrichs, R. *Phys. Chem. Chem. Phys.* **2005**, *7*, 3297. (b) Weigend, F. *Phys. Chem. Chem. Phys.* **2006**, *8*, 1057.

(27) (a) Schäfer, A.; Huber, C.; Ahlrichs, R. *J. Chem. Phys.* **1994**, *100*, 5829. (b) Eichkorn, K.; Weigend, F.; Treutler, O.; Ahlrichs, R. *Theor. Chem. Acc.* **1997**, *97*, 119.

(28) (a) Staroverov, V. N.; Scuseria, G. E.; Tao, J.; Perdew, J. P. *J. Chem. Phys.* **2003**, *119*, 12129. (b) Zao, Y.; Truhlar, D. G. *J. Chem. Theory Comput.* **2005**, *1*, 415. (c) Furche, F.; Perdew, J. P. *J. Chem. Phys.* **2006**, *124*, 044103.

(29) Staroverov, V. N.; Scuseria, G. E.; Tao, J.; Perdew, J. P. *J. Chem. Phys.* **2004**, *121*, 11507E.

(30) Jensen, K. P. *Inorg. Chem.* **2008**, *47*, 10357.

(31) McQuarrie, D. A. *Statistical Thermodynamics*; Harper & Row: New York, NY, 1973.

(32) Wiberg, K. B. *Tetrahedron* **1968**, *24*, 1083.

(33) Reed, A. E.; Weinstock, R. B.; Weinhold, F. *J. Chem. Phys.* **1985**, *83*, 735.

(34) Glendening, E. D.; Badenhoop, J. K.; Reed, A. E.; Carpenter, J. E.; Weinhold, F. *NBO 4.M*; Theoretical Chemistry Institute, University of Wisconsin, Madison, WI, 1999.

(35) Malkin, V. G.; Malkina, O. L.; Reviakine, R.; Arbuznikov, A. V.; Kaupp, M.; Schimmelpfennig, B.; Malkin, I.; Repiský, M.; Komorovský, S.; Hrobarik, P.; Malkin, E.; Helgaker, T.; Ruud, K. MAG-ReSpect program, version 1.2, University of Würzburg and Slovak Academy of Science; Germany and Slovakia, 2005.

(36) For further details, see: http://www.struked.de.